the FEBS Journal

Linking pseudouridine synthases to growth, development and cell competition

Giuseppe Tortoriello[1,*], José F. de Celis[2] and Maria Furia[1]

1 Dipartimento di Biologia Strutturale e Funzionale, Università di Napoli Federico II, Naples, Italy
2 Centro de Biologia Molecular Severo Ochoa, Universidad Autonoma de Madrid and Consejo Superior de Investigaciones Cientificas, Spain

Keywords
cell competition; dyskeratosis; *Notch*; pseudouridine synthase; snoRNP

Correspondence
M. Furia, Dipartimento di Biologia Strutturale e Funzionale, Università di Napoli Federico II, Complesso Universitario Monte Santangelo, via Cinthia, 80126 Naples, Italy
Fax: +39 081 679233
Tel: +39 081 679072; +39 081 679071; +39 081 679076
E-mail: mfuria@unina.it

***Present address**
European Neuroscience Institute at Aberdeen, University of Aberdeen, Aberdeen, UK

(Received 14 December 2009, revised 24 May 2010, accepted 3 June 2010)

doi:10.1111/j.1742-4658.2010.07731.x

Eukaryotic pseudouridine synthases direct RNA pseudouridylation and bind H/ACA small nucleolar RNA (snoRNAs), which, in turn, may act as precursors of microRNA-like molecules. In humans, loss of pseudouridine synthase activity causes dyskeratosis congenita (DC), a complex systemic disorder characterized by cancer susceptibility, failures in ribosome biogenesis and telomere stability, and defects in stem cell formation. Considering the significant interest in deciphering the various molecular consequences of pseudouridine synthase failure, we performed a loss of function analysis of *minifly* (*mfl*), the pseudouridine synthase gene of *Drosophila*, in the wing disc, an advantageous model system for studies of cell growth and differentiation. In this organ, depletion of the *mfl*-encoded pseudouridine synthase causes a severe reduction in size by decreasing both the number and the size of wing cells. Reduction of cell number was mainly attributable to cell death rather than reduced proliferation, establishing that apoptosis plays a key role in the development of the loss of function mutant phenotype. Depletion of Mfl also causes a proliferative disadvantage in mosaic tissues that leads to the elimination of mutant cells by cell competition. Intriguingly, *mfl* silencing also triggered unexpected effects on wing patterning and cell differentiation, including deviations from normal lineage boundaries, mingling of cells of different compartments, and defects in the formation of the wing margin that closely mimic the phenotype of reduced *Notch* activity. These results suggest that a component of the pseudouridine synthase loss of function phenotype is caused by defects in *Notch* signalling.

Introduction

Eukaryotic pseudouridine synthases comprise a highly conserved protein family, whose best characterized members are yeast Cfb5p, rat NAP57, and mouse and human dyskerin [1]. These proteins localize in the nucleolus and are involved in a variety of essential cellular functions, including processing and modification of rRNA [2], internal ribosomal entry site-dependent translation [3], DNA repair [4], nucleo-cytoplasmic shuttling [5] and, in mammals, stem cell maintenance and telomere integrity maintenance [6]. In archaeons

Abbreviations
A, anterior; *ap*, *apterous*; Cas3, caspase-3; DC, dyskeratosis congenita; D, dorsal; *en*, *engrailed*; FLP/FRT system, site-directed recombination system from the *Saccharomyces* 2 μ plasmid; GAL4, yeast galactose 4 activator protein; GFP, green fluorescent protein; LacZ, bacterial β-galactosidase; *mfl*, *minifly*; P, posterior; PH3, phosphohistone H3; rRNP, ribosomal ribonucleoprotein; RNAi, RNA interference; snoRNA, small nucleolar RNA; snoRNP, small nucleolar RNA-associated ribonucleoprotein; UAS, yeast upstream activation sequence; V, ventral; *wg*, *wingless*; X-DC, X-linked dyskeratosis congenita.

and all eukaryotes, members of the dyskerin family associate with small nucleolar RNAs (snoRNAs) of the H/ACA class to form one of the four core components of the H/ACA small nucleolar RNA-associated ribonucleoprotein (snoRNP) complexes responsible for rRNA processing and conversion of uridines into pseudouridines [1]. In the modification process, proteins of the dyskerin family act as pseudouridine synthases, and H/ACA snoRNAs select, via specific base-pairing, the specific residues to be isomerized [7,8]. In addition to rRNA, which represents the most common target, small nuclear RNAs, tRNAs or other RNAs can also be specifically pseudouridylated. Although pseudouridylation can contribute to rRNA folding, and ribosomal ribonucleoprotein (rRNP) and ribosomal subunit assembly, and can subtly influence ribosomal activity, the exact role of this type of modification still remains elusive. The crucial role of pseudouridine synthases as H/ACA snoRNA-stabilizing molecules [7,8] raises the possibility that their loss may also elicit a variety of pleiotropic effects related to a drop in snoRNA levels. This issue is of particular relevance, because H/ACA snoRNAs could act as potential microRNA precursors [9–13]. Besides participating in the formation of H/ACA snoRNPs, mammalian dyskerin associates with telomeric RNA, which contains an H/ACA domain, to form an essential component of the telomerase active complex [14]. Dyskerin is thus part of at least two essential but distinct functional complexes, one involved in ribosome biogenesis and snoRNA stability and the other in telomere maintenance. In humans, dyskerin is encoded by the *DKC1* gene [15], and its loss of function is responsible for X-linked DC (X-DC), a rare skin and bone marrow failure syndrome, and for Hoyeraal–Hreidarsson disease, now recognized as a severe X-DC allelic variant [16]. X-DC perturbs normal stem cell function, causes premature ageing, and is associated with increased tumour formation [6]. The distinction between the effects caused by telomere shortening and those related to impaired snoRNP functions is one of the main challenges posed by the pathogenesis of this disease. In this regard, *Drosophila* may represent an attractive model system with which to dissect the specific roles played by dyskerin in its two functionally distinct complexes.

The *Drosophila* homologue of dyskerin, encoded by the *Nop60B/minifly* (*mfl*) gene [17,18], is highly related to its human counterpart, sharing with it 66% identity and 79% similarity. The conservation increases remarkably within several specific domains, so that total identity exists between the *Drosophila* and human proteins within the two TruB motifs and the pseudouridine synthase and archaeosine transglycosylase RNA-binding domain, which are involved in the pseudouridine synthase activity. In addition, the most frequent missense mutations identified in X-DC patients fall in regions of identity between the human and the *Drosophila* genes. The *DKC1* and *mfl* genes also share a common regulatory network, as both are positively regulated by Myc oncoproteins [19,20], which play an evolutionarily conserved regulatory role in cell growth and proliferation during development [21,22]. Despite these similarities, telomere maintenance in *Drosophila* is not performed by a canonical telomerase, but by a unique transposition mechanism involving two telomere-associated retrotransposons, HeT-A and TART, which are attached specifically to the chromosome ends [23]. The striking conservation of rRNP/snoRNP functions, coupled with a highly divergent mechanism of telomere maintenance, makes *Drosophila* a valuable system in which to assess the roles specifically played by pseudouridine synthases in different functional complexes.

In previous genetic analyses, we showed that null mutations of *mfl* caused larval lethality, whereas flies carrying hypo-morphic mutations were viable, and caused a variety of defects, including developmental delay, defective maturation of rRNA, small body size, alterations of the abdominal cuticle, and reduced fertility [18]. However, the low vitality and fertility caused by the *mfl* hypomorphic allele impeded a detailed investigation of the molecular mechanisms that underlie its complex phenotype. We have now used RNA interference (RNAi) induced by the yeast galactose 4 activator protein (GAL4)/yeast upstream activation sequence (UAS) system to knock down gene expression in specific regions of transgenic flies. Given that formation of the *Drosophila* wing is an advantageous model system with which to study growth control and cell differentiation, we focused our analyses on the effects of loss of Mfl on the size and patterning of the wing. The results reported here indicate that *mfl* silencing affects organ dimensions mainly by reducing cell size and increasing apoptosis. Intriguingly, *mfl*-underexpressing cells exhibit a growth disadvantage and are progressively eliminated by cell competition in mitotic mosaics. Notably, other phenotypes associated with *mfl* knockdown mimic those caused by impaired *Notch* signalling, suggesting that Mfl pseudouridine synthase activity is required for the normal function of this conserved signalling pathway.

Results

RNAi expression

In previous molecular analyses, we showed that the *DKC1 Drosophila* orthologue (called *mfl*) encodes four

main mRNAs of 1.8, 2.0, 2.2 and 1 kb in length [18,24] (Fig. 1A). The three longer transcripts displayed identical coding potentials, differing from each other only at the level of their 3′-UTRs, whereas an alternative spliced 1.0 kb variant encoded a minor protein subform whose function remains, so far, elusive [24]. To reduce the expression of all mRNAs, we used a UAS silencing construct [25] targeting the exon 2–exon 3 junction, a sequence shared by all mRNAs (Fig. 1A). Two transgenic lines carrying an independent insertion of the construct, named *46279* and *46282* (Fig. 1B), were tested for silencing efficiency upon ubiquitous RNAi expression driven by the *act5c–GAL4* driver. Under these conditions, eclosion or formation of pharate adults was never observed, and severe developmental delay and larval lethality occurred in both strains. However, the lethal phase differed, as most of the *46282*-silenced progeny died as first instar/second instar larvae (Fig. 1C), whereas some *46279*-silenced larvae developed up to the third instar, although with a significant delay (6–7 days). However, none of these latter progeny pupariated, and most of them showed multiple melanotic tumours (Fig. 1D). Larval melanotic tumours are not believed to be neoplastic, but are thought to arise as a result of immune responses to cells and tissues that are incorrectly differentiated, or from haematopoietic cells that overgrow during the third larval instar stage [26,27]. To further define the silencing efficiency of the RNAi constructs, total RNA was isolated from *46282*-silenced and *46279*-silenced larvae and their controls, and the amounts of *mfl* transcripts were determined by real-time RT-PCR experiments. Both silenced progenies showed a significant drop in *mfl* transcript levels (Fig. S1), with the higher loss corresponding to a combination that displayed an earlier lethal phase (*46282/act5c–GAL4*). These data indicated that survival is generally related to the level of *mfl* transcripts, confirming the previously described dose effects of *mfl* alleles [18]. As both phenotypic and molecular data indicated that the *46282* line exhibited the most marked silencing effect, this strain was used in subsequent experiments. Even though this strain was predicted to have high silencing specificity and no off-targets (see http://stockcenter.vdrc.at), we utilized two additional VDRC lines carrying a different UAS silencing construct [25] in order to completely rule out the possibility that the observed effects could be caused by silencing of an independent gene. The two lines, named *34597* and *34598*, exhibited a silencing

A

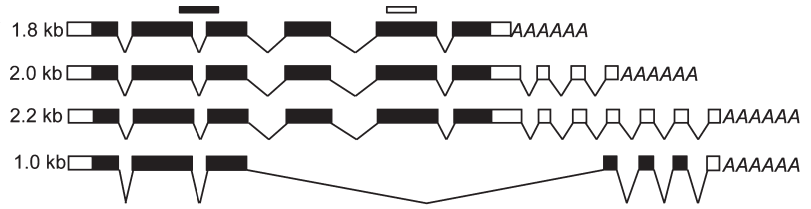

B

Strain	Construct #	Inserted Chromosome	Target on *mfl* gene
46 279	16 822	2	Exon 2–3 junction
46 282	16 822	2	Exon 2–3 junction
34 597	10 940	3	Exon 5
34 598	10 940	2	Exon 5

C D

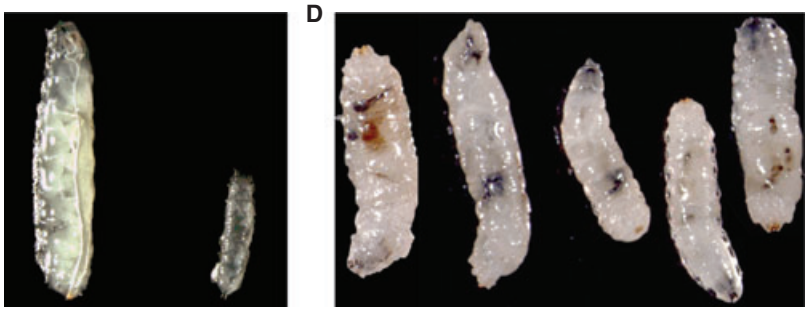

+/act-GAL4 (6 days) 46282/act-GAL4 (6 days) 46279/act-GAL4 (12 days)

Fig. 1. Structure and expression of *mfl*-silencing constructs. (A) Schematic structure of the four *mfl* mRNA isoforms [24]; coding regions are in black. The black bar on the top shows the position of the DNA segment employed in the *16822* VDRC RNAi construct [25], which targets all mRNA isoforms, and the open bar shows the position of the DNA segment employed in the *34597* and *34598* VDRC RNAi strains [25], which is unable to target the 1.0 kb variant mRNA. (B) Main properties of the *46279* and *46282* transgenic lines, each carrying an independent insertion of the *16822*-silencing transgene on chromosome 2, and of the *34597* and *34598* lines, each carrying an independent insertion of the *10940*-silencing transgene on chromosomes 3 and 2, respectively. (C, D) Phenotypes generated by RNAi-mediated silencing in larvae of *46282/act–GAL4* and *46279/act–GAL4* genotypes.

efficiency weaker than that displayed by the *46282* strain, possibly because the silencing construct was unable to target the alternative spliced 1.0 kb variant mRNA (Fig. 1A). However, although at lower penetrance and expressivity, the phenotypes obtained in the *46282* strain were similarly observed in both the *34597* and *34598* lines.

Loss of Mfl pseudouridine synthase affects both size and morphogenesis of the developing wing

To overcome the lethality induced by ubiquitous silencing, we focused our analyses on the developing wing, which represents an excellent and well-characterized model for the study of organogenesis. The effects caused by depletion of the Mfl pseudouridine synthase were dissected by driving RNAi expression in different wing territories. The *GAL4* lines used in these experiments, their expression profile in the wing and the summary of the overall effects elicited are shown in Fig. 2. When silencing was directed by the *nub–GAL4* driver, which triggers RNAi in the whole wing blade and hinge, we observed a 45% average reduction in wing size. Intriguingly, only 10–20% of these small wings were correctly patterned, and most showed moderate or severe developmental defects. These defects were variable, ranging from ectopic or irregular vein formation and wing blisters to complete disorganization of the wing blade, which appeared crumpled or vestigial (Fig. 2A). Silencing directed by *MS1096–GAL4* (which drives RNAi in the dorsal (D) compartment of the wing disc earlier, and more broadly throughout the developing wing pouch later [28]) caused markedly stronger defects, consisting in severe wing malformations with complete penetrance. As shown in Fig. 2B, these wings showed absent or irregular margins and were often strongly underdeveloped and highly disorganized, phenocopying a severe vestigial-like phenotype. As expected, wing undergrowth was more marked in the D compartment, such that the blades curved upwards, and lack of adhesion between the D and ventral (V) wing surfaces caused frequent formation of blisters (Fig. S2). Notably, these effects were occasionally asymmetrical, with one wing strongly deformed and the other less affected, and in most cases the phenotypes were more severe in males than in females (not shown). The main defects triggered by the *vg–GAL4* driver, which activates RNAi at the D–V boundary, were incomplete and notched margins with variable scalloping of the wing blade, and loss or irregular patterning of the margin bristles (Fig. 2C). Again, the phenotype was occasionally asymmetrical, with only one wing exhibiting strong abnormalities. The *engrailed* (*en*)*–GAL4* driver triggered *mfl* silencing specifically in the posterior (P) compartment. Wing abnormalities were thus essentially restricted to the P sector, and included a significant reduction of this area, notches and loss of hairs at the

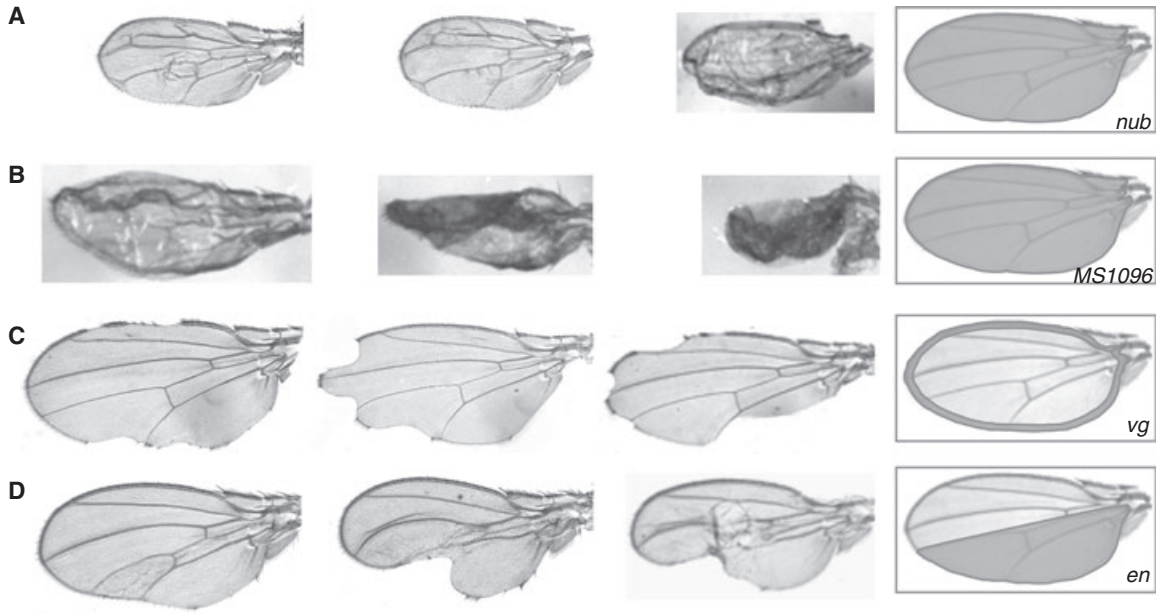

Fig. 2. Adult wing phenotypes generated by RNAi-mediated *mfl* silencing. RNAi was activated by *nub–GAL4* (A), *MS1096–GAL4* (B), vg^{BE}–*GAL4* (C) and *en–GAL4* (D) drivers, whose expression profiles in the wing are depicted on the right. Phenotypes were highly variable, ranging from mild (left) to more severe defects (right).

P margin, and alterations in the position of the P veins (Fig. 2D). Strong disorganization of the whole wing blade, mimicking a vestigial-like phenotype, was also observed in about 30% of these flies. All together, the results obtained with different *GAL4* driver lines indicated that *mfl* silencing not only affects wing size, but also causes a variety of morphogenetic defects affecting wing development. Although present at lower penetrance and expressivity, similar phenotypes were observed after *mfl* silencing in the *34597* and *34598* lines (Fig. S3).

mfl regulates organ size by affecting the size and the number of cells

To determine whether the reduced wing size of *mfl* knockdown flies resulted from a decrease in the size and/or in the number of cells, we performed different morphometric analyses (see Experimental procedures). In these experiments, *nub–GAL4*-silenced and *en–GAL4*-silenced flies showing mild patterning defects were chosen, and their total wing area, anterior (A) and P compartments area and cell density were measured (see Experimental procedures). Cell size was then estimated as the inverse of cell density. Loss of Mfl in the P compartment (*46282/en–GAL4*) resulted in a nearly 20% reduction in wing size as compared with controls (Fig. 3A,B,F). As expected, this reduction was mostly restricted to the P compartment, as confirmed by the significant increase in the A/P compartment ratio (Fig. 3F). The numbers of cells were almost identical in standard square areas from the A and P compartments, indicating that cell size was normal (Fig. 3H). Hence, the reduction in the P compartment might arise from reduced proliferation or from increased cell death (see next paragraph). The total wing area was reduced by 45% in knockdown flies of the *46282/nub–GAL4* genotype, with the A and P compartments contributing identically to this drop (Fig. 3C,D,G). However, in this case, the diminution of wing size was accompanied by a decrease in cell size (Fig. 3H). Taken together, these results indicated that loss of Mfl can affect both cell size and number. The relative contribution of these effects to wing size may depend on the strength of the *GAL4* driver and/or the domain of RNAi expression. Indeed, it is reasonable to suppose that weak silencing may only affect cell size, whereas strong silencing may lead to apoptosis. Alternatively, the effects may depend on the mutant area [29]. In fact, the loss of wing tissue and the drop in cell numbers observed in the silenced compartment of *46282/en–GAL4* wings may derive from the confrontation along the A–P compartment boundary of cells with different levels of *mfl* expression. To better evaluate the role played by Mfl in viability, growth and differentiation of cells, we then extended our analyses to earlier developmental stages, looking at the developing wing disc.

mfl silencing impairs compartment boundary formation

The wing disc is subdivided into A, P, D and V compartments by lineage restriction boundaries [30,31]. This allowed us to limit the expression of Mfl to specific domains, thus defining the responses of definite territories of cells to its depletion. The expression of Mfl in wild-type discs is ubiquitous and localized to the nucleoli, as previously observed in other tissues [18] (Fig. 4A). In discs subjected to *mfl* silencing in the P compartment (marked by the expression of the *UAS–GFP* transgene; see Fig. 4B), strong and localized Mfl depletion was observed. Intriguingly, in these discs, the A–P boundary, depicted by the edge of green fluorescent protein (GFP) expression, appeared irregular and deformed (Fig. 4B). This defect cannot simply be explained on the basis of growth perturbation, as previous studies on *Minute* mutations, which affect ribosome components [32,33], indicated that different relative growth rates of the A and P compartments do not perturb compartment boundary formation [29,32]. We then checked the expression of key patterning regulatory genes in the silenced discs. To check the activity of the *Notch* pathway, which is implicated in the control of a variety of cellular processes, including cell proliferation, cell fate specification, and determination of the compartment affinity boundary [34–36], we followed the expression of the *wingless* (*wg*) gene, known to be a major *Notch* target, in patterning of the wing margin. In wild-type discs, signalling between V and D cells resulted in the formation of a band four or five cells wide at the D–V border, which was marked by a central stripe of *wg* expression (Fig. 4C). Notably, staining of *46282/en–GAL4*-silenced discs with specific antibody against Wg showed also that the D–V margin was undulatory and distorted (Fig. 4C). Thus, the first effect elicited by localized *mfl* silencing in the developing disc appears to be a deformation of normal lineage boundaries. Consistent with the results obtained by morphometric analysis, when *46282/en–GAL4*-silenced wing discs were labelled with antibody against activated caspase-3 (Cas3), localized apoptosis was observed in the P compartment (Fig. 5A,A′). In contrast, staining of mitotic cells with antibody against phosphohistone H3 (PH3) did not show a significant decrease in cell division (Fig. 5B,B′).

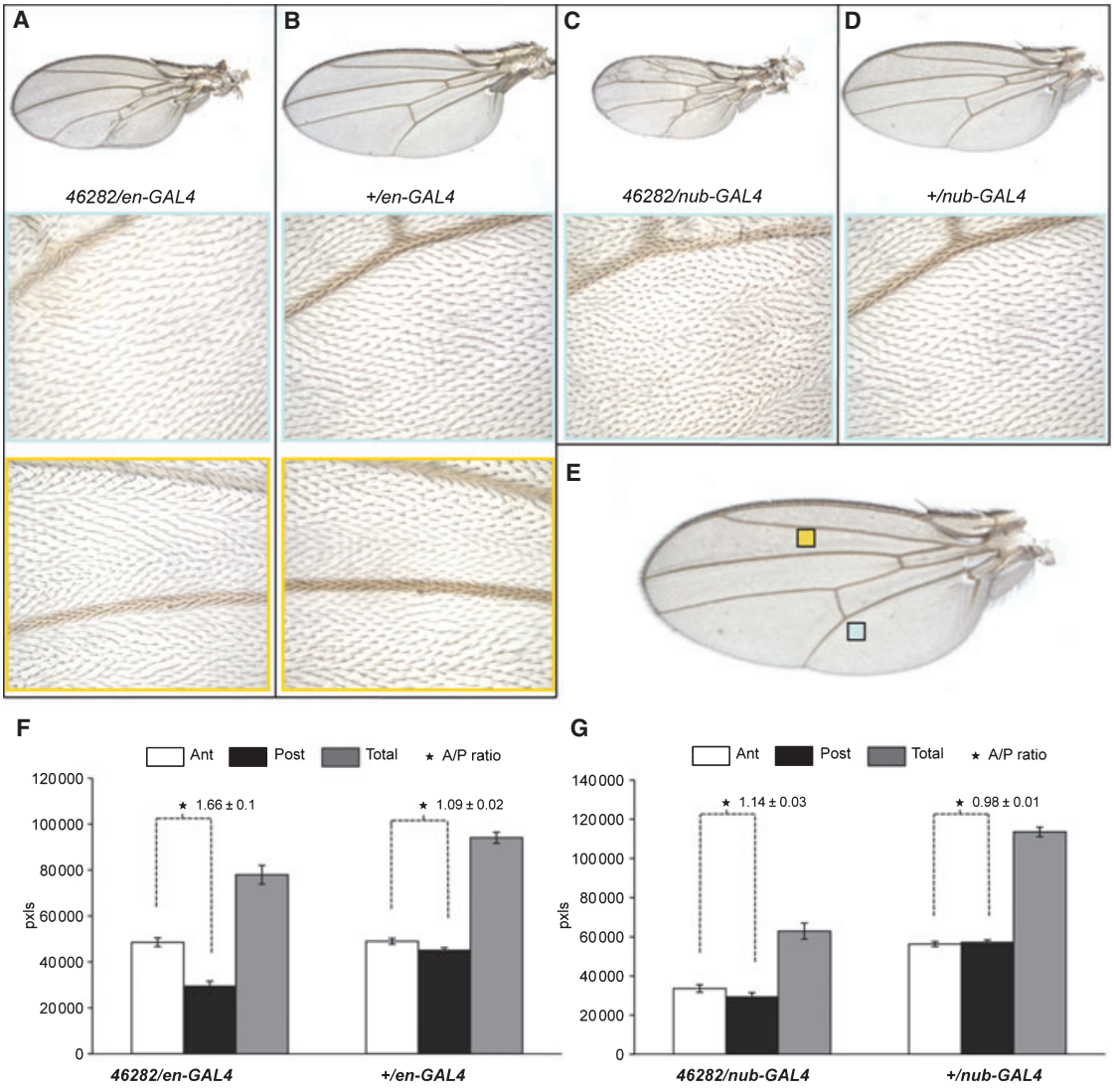

H

	46282/en-GAL4	*+/en-GAL4*	*46282/nub-GAL4*	*+/nub-GAL4*
Cell density posterior comp. (cell • 0.25 mm^{-2} ± SD)	19.3 ± 2.8	19.1 ± 1.1	36.0 ± 2.9	17.4 ± 1.4
Cell size posterior comp. (mm^2)	0.01295	0.01309	0.00694	0.01437
Cell density anterior comp. (cell • 0.25 mm^{-2} ± SD)	21.8 ± 1.8	23.4 ± 1.1	37.8 ± 1.7	18.1 ± 2.0
Cell size anterior comp. (mm^2)	0.01147	0.01068	0.00661	0.01381

Fig. 3. Organ and cell size adult phenotypes produced by *mfl* silencing. Wings of *46282/en–GAL4* and *46282/nub–GAL4* male adult flies (A, C) and their *+/en–GAL4* and *+/nub–GAL4* respective controls (B, D) were analysed to determine total wing area, size of A and P compartments, and their ratio (A/P). Cell number was calculated by counting the number of tricomes (each cell has a single tricome) for the selected area of each compartment, shaded in orange for the A compartment and in azure for the P compartment (E). The number of cells within a standard square allowed us to calculate the cell density. Induction of *mfl* silencing in the P compartment by the *en–GAL4* driver specifically reduced this sector of the wing blade, leading to a significant increase in the A/P ratio (F). Ubiquitous silencing directed by *nub–GAL4* reduced the size of the whole wing size without significantly affecting the A/P ratio (G). Cell density, reported in (H), indicates the average number of cells counted in a standard square of 0.25 mm^2; SD, standard deviation. Note the marked increase in cell density occurring in wings of the *46282/nub–GAL4* genotype but not in those of the *46282/en–GAL4* genotype. This indicates that final wing size is regulated by reducing cell dimensions in *46282/nub–GAL4* flies but not in *46282/en–GAL4* flies.

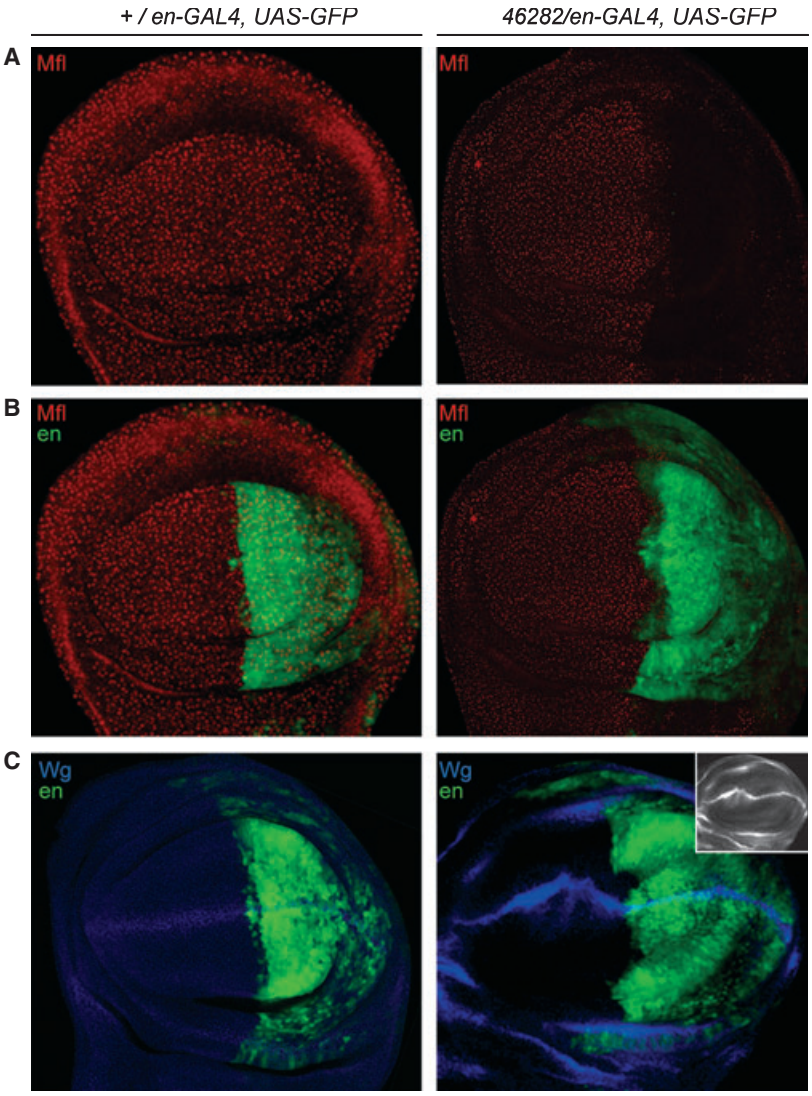

Fig. 4. Depletion of Mfl affects the shape of compartment boundaries in the wing disc. (A) In wild-type third instar wing discs, Mfl (red) is expressed ubiquitously and localizes in the nucleolus (left). In *46282/en–GAL4* discs, RNAi specifically triggered in the P compartment (green, GFP-labelled in B) elicits strong and localized Mfl depletion (right). (B) A strong deformation of the A–P compartment boundary is observed in the silenced discs (right) as compared with the control (left). (C) The D–V compartment border, marked by the central stripe of Wg expression (blue; white in the inset) was also found to be deformed and undulatory upon *mfl* silencing (right), indicating that Mfl depletion perturbs both the A–P and D–V boundaries.

In the *34597* and *34598* strains, *mfl* silencing in the D compartment under the control of the *apterous* (*ap*)–*GAL4* driver led to larval lethality, although a few adult escapers exhibiting notum and/or wing defects highly reminiscent of defective *Notch* signalling (Fig. S3) were recovered. No adults of the *46282/ap–GAL4* genotype were recovered, but the larval wing discs, although smaller and abnormal in shape, were still amenable to immunostaining analyses. The expression domain of *GAL4*, marked by the *UAS–GFP* reporter, was strictly coincident with the region in which Mfl was depleted (Fig. 6A,B). Remarkably, in these discs, the edge of the D–V boundary was again irregular (Fig. 6B). As in wild-type discs (Fig. 6C), Wg expression strictly followed the D–V margin, although this was highly deformed (Fig. 6D,E). Moreover, in late third instar discs, patches of boundary cells started to detach from the irregular D–V border, becoming surrounded by V cells (Fig. 6E). Discontinuous and irregular formation of the D–V margin was similarly observed after *mfl* silencing in the *34597* and *34598* lines (Fig. S3), leading us to exclude the occurrence of off-target effects. All together, these observations further confirm that *mfl* downregulation strongly disturbs the shape of the boundary and affects *Notch* signalling and *wg* expression. Although the most simple explanation for these results is that *Notch* signalling requires high levels of protein synthesis, we noticed that a canonical Brd-box, a typical hallmark of *Notch* target genes [37], is present within the 3′-UTR of the two longer *mfl* transcripts (Fig. S4). Thus, although more direct evidence is required, it cannot be excluded that *mfl* may represent a direct target of the *Notch* regulatory cascade.

Taking advantage of the strong silencing exerted by the *ap–GAL4* driver in the *46282* genotypic context, we

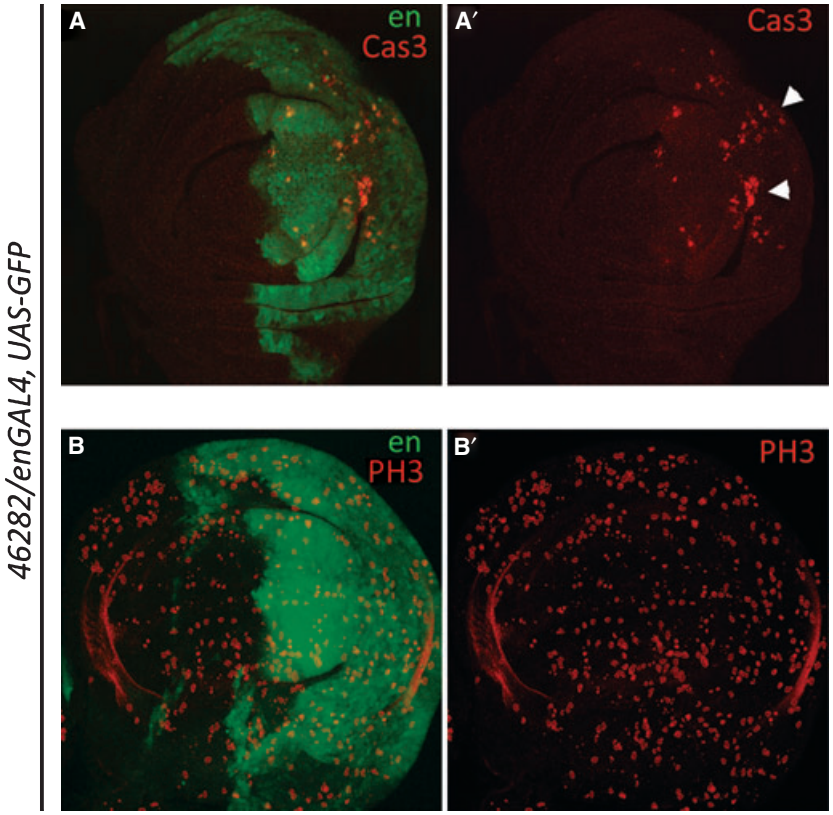

Fig. 5. Effects of *mfl* silencing on apoptosis and cell proliferation in the wing disc. (A, A′) *mfl* silencing in the P compartment, under control of the *en–GAL4* driver, causes significant induction of apoptosis in the silenced compartment (marked by the *UAS–GFP* reporter), as visualized by staining with antibody against activated Cas3 (red). (B, B′) In contrast, staining with antibody against PH3 (red) to visualize mitotic cells did not show a significant alteration of the proliferative rate in the P compartment (marked by the *UAS–GFP* reporter; see also Fig. S5B).

investigated whether *mfl* underexpression in the D compartment affected cell proliferation and/or apoptosis more significantly. In control discs, the average numbers of dividing cells were similar in the D and V compartments. Instead, in the silenced discs, the proliferation rate was, on average, reduced by about 14% in the D (silenced) compartment as compared with the V (unsilenced) compartment (Figs 6F and S5). This reduction is quite modest, suggesting that apoptosis could be the main contributor to the loss of function *mfl* phenotype. The localized increase in apoptosis may be an indirect consequence of abnormal compartment boundary formation, which in turn may derive from defects in cell adhesion and/or cell communication.

mfl silencing triggers apoptosis and sorting out of D cells towards the V compartment

To assess the specific effects on cell apoptosis, *ap–GAL4,UAS–GFP* silenced-discs were stained with antibody against activated Cas3. These experiments revealed a dramatic effect in late third instar wing discs, where Cas3 labelling revealed large areas of apoptotic foci. Remarkably, these foci correspond to D (GFP-labelled) cells that crossed the D–V boundary, becoming embedded in the V compartment (Fig. 7). This indicated that the silenced cells, albeit retaining D identity, failed to maintain stable interactions with other D cells and sorted-out towards the V compartment. This conduct is compatible with invasive migratory behaviour, possibly acquired as consequence of loss of specific affinity for the proper compartment or, alternatively, with progressive displacement of the dying D cells by the faster-growing V cells. Considering that correct formation of the D–V boundary normally prevents mingling of D and V cells, it seems reasonable to conclude that in the silenced discs the irregular and defective formation of the D–V border is caused by defective cell–cell interactions, which, in turn, may lead to apoptosis. Remarkably, RNAi-mediated silencing of *DKC1*, the human orthologue of *mfl*, has similarly been reported to induce lack of adhesion of cultured cells [38].

mfl activity is involved in cell competition

To further define the effects of loss of Mfl on cell survival, we used mosaic analysis to induce clones homozygous for mfl^{05}, a loss of function mutation causing larval lethality [18]. Site-specific mitotic recombination was induced by means of the site-directed recombination system from the *Saccharomyces* 2 μ plasmid

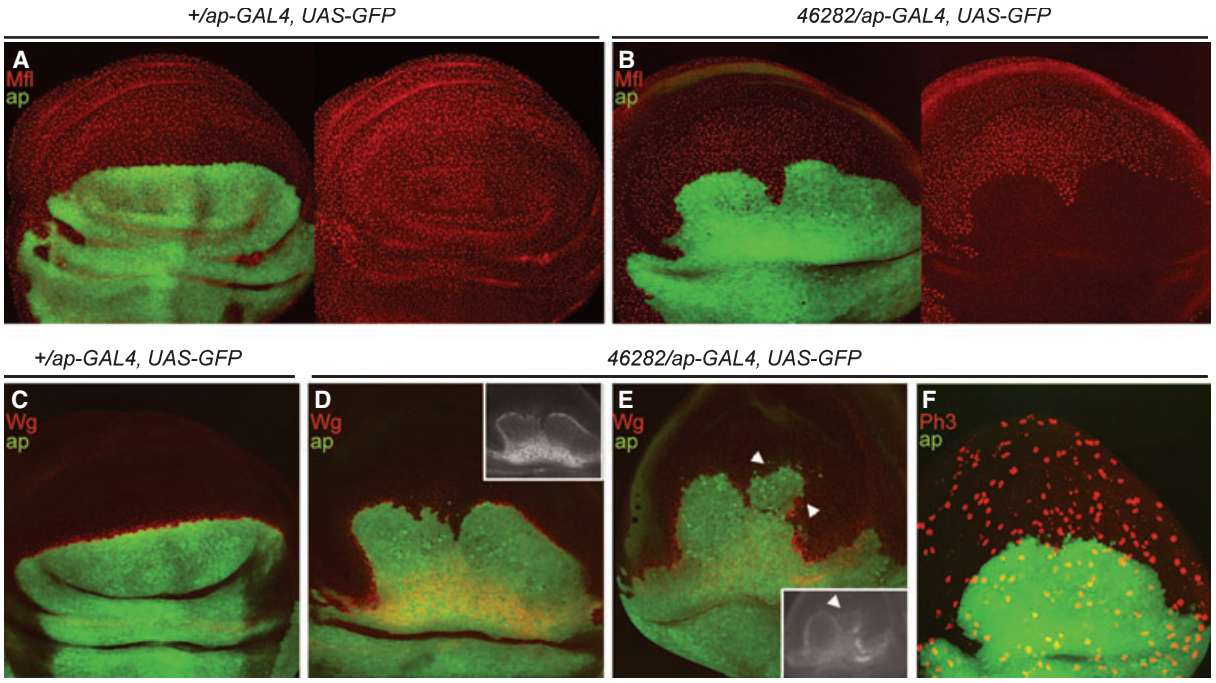

Fig. 6. Depletion of Mfl reduces cell proliferation and causes strong deformation of the D–V boundary. Expression of Mfl (red) in wing discs from control (A) or *46282/ap–GAL4*-silenced larvae (B). The domain of the expression of the *ap–GAL4* driver, restricted to the D compartment, is GFP-labelled (green). The strong and localized depletion of Mfl in the D compartment is accompanied by a marked deformation of the D–V boundary. The central stripe of Wg expression (red) strictly follows the D–V border in both control (C) and silenced (D, E) discs. This can be more clearly observed in the insets, where Wg expression (white) is shown alone. Note that in late third instar silenced discs, patches of D cells detach from the irregular D–V border (E; see arrow). When stained with antibody against PH3 (red) to visualize mitotic cells, the silenced compartment showed a modest reduction of the proliferative rate (F) (see also Fig. S5A).

(FLP/FRT) system [39], and the wing discs were analysed for the presence of homozygous mutant cells. Mutant clones were first generated in a *Minute* background, by heat-inducing FLP recombinase in $M^{+/-}$ heterozygous larvae (see Experimental procedures). *Minute* mutations affect protein synthesis and are characterized by recessive cell lethality and by a dominant growth defect [32]. As heterozygous $M^{+/-}$ cells, although viable, are delayed in their development and take longer to reach their normal size, this background furnishes a favourable context to facilitate the survival and growth of clones homozygous for a deleterious mutation. In these experiments, mutant clones were marked by the absence of bacterial β-galactosidase (LacZ), whereas twin clones homozygous for the *Minute* mutation could not produce proteins and died. At 48 h after induction, mfl^{05} cells were viable and capable of covering large areas of the disc (Fig. 8A), indicating that the mfl^{05} mutation is not lethal at the cellular level. Large mutant clones that originated early, before the establishment of the D–V border, abutted this margin, leaving its shape locally unaffected, as demonstrated by the normal pattern of Wg expression in D–V edge cells (Fig. 8A). These observations supported the hypothesis that deformation of compartment boundaries could be caused by juxtaposition of cells expressing different amounts of Mfl along the borders, and suggested that a *Minute* background might furnish a homotypical environment in which mfl^{05} cells may compensate for their growth defect. We therefore attempted to recover mutant clones in the adult wings. To this aim, mosaics were generated in larvae of the *hs*FLP1.22, f^{36a}; FRT42D, f^{+}, *M(2)l2/* FRT42D, mfl^{05} genotype, in order to associate the expression of the mfl^{05} mutation with that of the *forked* marker, which affects the shape of adult tricomes. Surprisingly, the frequency and size of f^{36a}, mfl^{05} clones were strongly reduced as compared with those of f^{36a} clones from the *hs*FLP1.22, f^{36a}; FRT42D, f^{+}, *M(2)l2/*FRT42D control strain (Fig. 8B). As large mfl^{05} clones were recovered in the wing disc, we concluded that viability of mutant cells decreased during development, and that the fitness of mfl^{05} cells was suboptimal even in a *Minute* background. Intriguingly, reduced fitness was accompanied by developmental abnormalities at the wing margin, where mutant clones

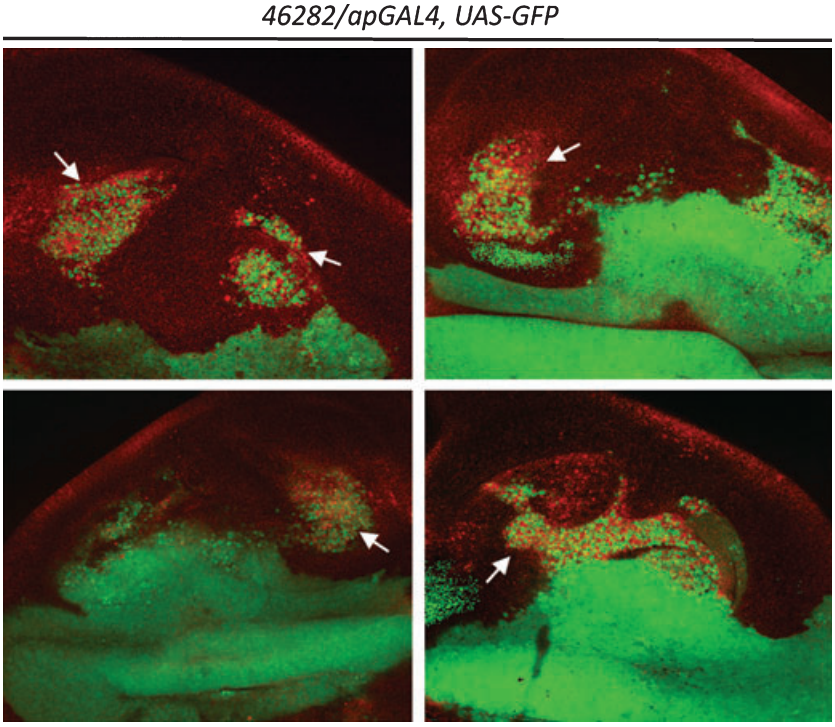

Fig. 7. Depletion of Mfl triggers apoptosis coupled with sorting-out cell behaviour. To better evaluate the effects of Mfl depletion on cell apoptosis, late third instar *46282/ap–GAL4*-silenced discs were stained with antibody against activated Cas3 (red) to visualize apoptotic cells. As is evident, Cas3 staining revealed large areas of apoptotic cells localized in the V (unsilenced) compartment. These apoptotic foci were composed of GFP-labelled dorsal cells, possibly displaced from the D compartment as a consequence of defective differentiation.

were often surrounded by generalized disorganization of the adjacent tissue. Two examples are reported in Fig. 8, which shows a clone at the P wing margin, closely flanked by a bifurcation of vein L5 and by transversal wing fractures (Fig. 8C), and a clone at the A wing margin, surrounded by marked disorganization of the flanking area (Fig. 8D). This picture hints at the possibility that cells surrounding the mosaic sector may not differentiate properly, perhaps as consequence of the confrontation between cells expressing different levels of Mfl or still unexplained cell nonautonomous effects, such as defects in cell communication and/or cell affinity.

In order to evaluate the growth of mfl^{05} cells in a context allowing twin clone analysis, we induced the formation of clones homozygous for mfl^{05} in a wild-type genetic background (see Experimental procedures). In these experiments, mfl^{05} clones were recognized by lack of GFP expression, whereas wild-type twins had double the amount of GFP expression as that on the heterozygous background. Remarkably, in this genetic context, mfl^{05} clones were completely missing or their size was greatly reduced as compared with twins (Fig. 9A,B). Thus, mutant cells are severely disadvantaged and eliminated from the epithelium when surrounded by heterozygous wild-type cells. As the occurrence of context-dependent cell survival is the main hallmark that distinguishes cell competition from other processes that involve cell death, this finding strongly supports the conclusion that variations in *mfl* expression levels can actually trigger cell competition.

Discussion

Loss of *mfl*-encoded pseudouridine synthase confers a growth disadvantage on cells and triggers apoptosis

We used the *GAL4–UAS* system to silence the *mfl* gene by RNAi *in vivo*, in the developing wing disc. We found that *mfl* silencing directed by a variety of different drivers was always able to elicit a region-specific size reduction in the corresponding domains of *GAL4* expression. The size reduction was achieved by decreases in cell size and cell number, depending on the *GAL4* driver used. A significant effect on cell size was manifested in the wing pouch, where *mfl* silencing led to markedly higher cell density. Conversely, a decrease in cell number was observed upon silencing in the P and D compartments. This effect was mainly caused by cell death rather than reduced proliferation, indicating that apoptosis is a major component of the loss of function mutant phenotype. As induction of apoptosis has been previously described in the ovaries of *Drosophila mfl* hypomorph mutants [18] or after localized RNAi in the notum [40], it can be concluded that it represents a general consequence of strong Mfl loss. Growth defects caused by Mfl depletion were

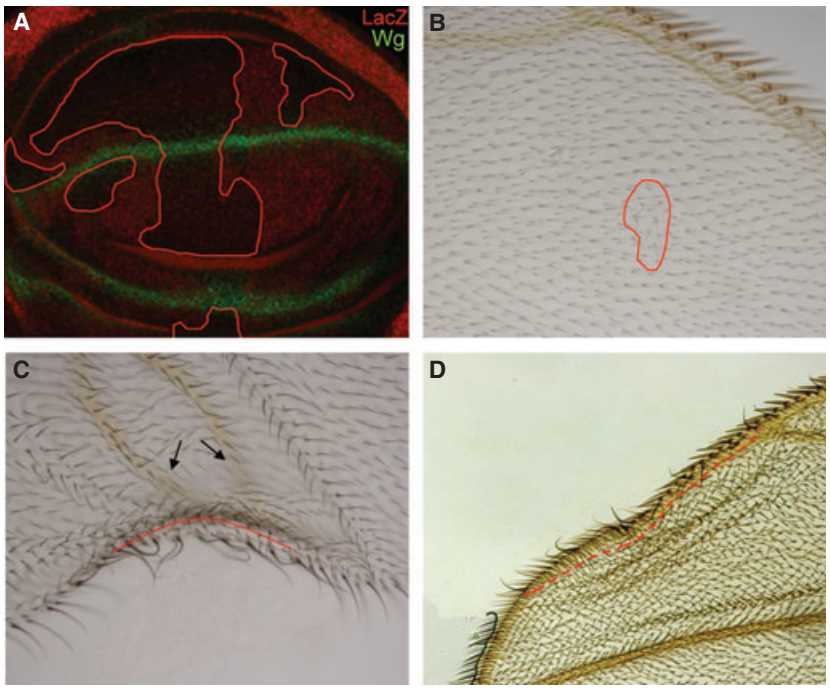

Fig. 8. Mosaic analyses of clones homozygous for the *mfl*^{05} lethal mutation in the *Minute* background. (A) FLP/FRT-mediated site-specific mitotic recombination was heat-induced in heterozygous larvae of the *hs*-FLP1.22; FRT42D, *mfl*^{05}/FRT42D, *arm*-LacZ, *M(2)l2* genotype to allow mosaic analysis in the wing disc. Mutant clones were recognized by lack of LacZ (red). At 48 h after induction, *mfl*^{05} cells (surrounded by the red line) were viable and occupied large areas of the developing wing disc. Note that the central stripe of Wg expression (green) that marks the D–V boundary appears to be normally shaped. (B–D) To follow the presence of *mfl*^{05} clones in the later stages of development, mitotic recombination was heat-induced in heterozygous larvae of the *hs*-FLP1.22, *f*^{36a}; FRT42D, *f*$^{+}$, *M(2)l2*/FRT42D, *mfl*^{05} genotype, and recombinant clones were detected in the adult wings by expression of the *f*^{36a} marker. (B) These clones constituted only a small fraction of the lamina, indicating that, even in the *Minute* context, the presence of the *mfl*^{05} mutation decreased cell viability during development. In addition, clones adjacent to the wing margin showed developmental defects in the flanking areas, such as L5 vein bifurcation (C), or generalized disorganization of the surrounding tissues (D).

further analysed by mosaic analyses. Although viable, mutant clones homozygous for the *mfl*^{05} lethal allele were disadvantaged even in the *Minute* background, and strongly outcompeted by wild-type cells. Thus, cells expressing lower levels of Mfl have a growth disadvantage that leads to their elimination by cell competition, a key mechanism by which cells are able to coordinate different rates of growth and apoptosis [41]. Only a few *Drosophila* mutations, in addition to *Minute*, are able to trigger cell competition [42]. Among these, *d-myc* alleles constitute the best known example, as mutations reducing *d-myc* expression cause cell elimination in mosaics, whereas cells overexpressing *d-myc* outcompete normal cells [43,44]. Intriguingly, *d-myc* hypomorph alleles lead to formation of small flies [45] whose phenotype is highly reminiscent of that caused by *mfl* mutations [18]. Considering that *mfl* is a target of d-Myc in the wing disc in microarray experiments [19], it is likely that it may mediate several aspects of the *d-myc* wing phenotype.

A novel role for the Mfl pseudouridine synthase – linking tissue growth to developmental events

One important aspect of organ size control is how the regulation of cell growth, proliferation and death is integrated with signalling pathways that regulate the organ's developmental program. It is, then, particularly relevant that localized *mfl* silencing not only induces a regional reduction in the size of the silenced territory, but also affects the formation of compartmental boundaries and disturbs wing morphogenesis. The finding that *mfl* silencing causes phenotypes highly reminiscent of those resulting from defective *Notch* signalling and strongly perturbs the formation of the D–V boundary and *wg* expression is particularly interesting, as it provides new insights into the mechanisms by which pseudouridine synthases may coordinate growth with developmental programs. During wing development, delineation of the D–V boundary is controlled by the *Notch* pathway, whose impairment leads

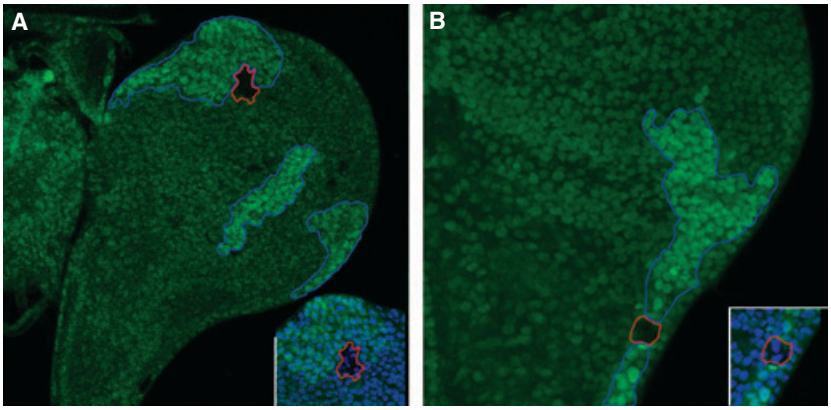

Fig. 9. Twin mosaic analyses of clones homozygous for the *mfl*^{05} lethal mutation. To perform twin clone analyses, FLP/FRT-mediated site-specific mitotic recombination was heat-induced in heterozygous larvae of the *hs*-FLP1.22; FRT42D, P[Ubi-GFP]/FRT42D, *mfl*^{05} genotype. *mfl*^{05} mutant clones, marked by the red line, were recognized by lack of GFP expression, whereas wild-type twin clones (marked by the blue line) had double the amount of GFP expression as seen in the heterozygous background. Remarkably, at 48 h after induction, *mfl*^{05} clones were missing or their size was substantially reduced as compared with twins, indicating that they were severely disadvantaged and eliminated by cell competition. To check that cells that did not show GFP expression were not in a different focal plane, the nuclei were visualized by 4′,6-diamidino-2-phenylindole staining (shown in the insets, bottom right).

to both decreased proliferation and cell affinity changes [35]. Although the possibility cannot be excluded that reduced expression of Wg may represent a secondary effect, as it may be correlated with a reduction in the number of *wg*-expressing cells at the D–V boundary, it is intriguing to note that a strong dependence of *Notch* activity on the level of ribosome synthesis during wing development has been suggested by several authors, suggesting that a cooperative effect between *Notch* and *Minute* mutations is required during wing formation [46–49]. Loss of the Nopp140 ribosome assembly factors also cause developmental wing defects, such as notched margins and blister formation [50]. Our results further support the idea that *Notch* signalling in the developing wing is hypersensitive to translational deficits. However, the finding that the Mfl pseudouridine synthase may act as an effector of *Notch* signalling may be of more general relevance, as *Notch* controls cell differentiation in many tissues, regulating binary cell fate decisions and stem cell maintenance [51].

The development roles of pseudouridine synthases and their implications for the pathogenesis of X-DC

Dyskerin, the human pseudouridine synthase, has conserved functions in ribosome biogenesis and snoRNP formation, and plays additional roles in telomere maintenance [1]. In the pathogenesis of X-DC, the regulation of telomere stability is usually considered to be prevalent, and is thought to be the main cause of the growth defects observed in proliferative tissues. Consequently, the disease is commonly regarded as a 'telomere and stem cell dysfunction' [6]. Although this interpretation is further supported by the observation that mutations in genes encoding other telomerase components may cause DC autosomal forms, the fact that X-DC is more severe strongly suggests that other dyskerin functions contribute to the disease. This view has recently been strengthened by the findings that dyskerin pathogenic mutations dramatically affect its interaction with a novel H/ACA snoRNP assembly factor [52].

The data reported here provide new insights into the mechanisms by which the dyskerin rRNP/snoRNP functions could account for the peculiar severity of X-DC. In this regard, we consider particularly relevant the possibility that, as occurs in *Drosophila*, mammalian pseudouridine synthases might be involved in crucial developmental processes, such as *Notch* signalling and cell competition. *Notch* activity is, in fact, essential to preserve the stem cell/progenitor cell balance, and its aberrant expression can promote, or abrogate, cancer development in a context-dependent manner [51]. Thus, integration of the *Notch* pathway with ribosome biogenesis during development may potentially account, at least partially, for dyskerin involvement in stem cell maintenance and cancer, two aspects that have so far been related exclusively to its role in telomere stability. Cell competition is also instrumental in stem cell maintenance, as well as in ageing and tumour development [53], all of which are affected by DC. As this process is conserved in mouse tissues [54], it is likely that a cell

competition-like process is responsible for the growth disadvantage caused by dyskerin pathogenic mutations in female heterozygous mice. In these females, extreme skewing of X-inactivation was observed even in the absence of telomere shortening, with most heterozygous cells showing an active wild-type X-chromosome [4,55]. This implies that cells expressing the dyskerin-mutated allele were disadvantaged and did not survive, as a consequence of a cell competition-like effect. Although this effect is thought to depend exclusively on the interaction of dyskerin with telomerase [4], failure of dyskerin rRNP/snoRNP functions may make a substantial contribution to it, by triggering progressive elimination of disadvantaged cells by apoptosis. Indeed, the possibility that relative differences in rRNP/snoRNP functions can trigger cell competition may indicate a novel role for metazoan pseudouridine synthases in interlacing cell growth and development.

Finally, recent data showing that snoRNAs may act as microRNA precursors [9–13] suggests additional mechanisms by which pseudouridine synthase depletion may affect developmental processes. Loss of pseudouridine synthases might, in fact, inhibit the snoRNA-derived microRNA pathway, thereby widely disturbing metazoan development. It is tempting to suggest that this mechanism might possibly account, at least in part, for the plethora of manifestations displayed by X-DC.

Experimental procedures

Drosophila strains

Flies were raised on standard *Drosophila* medium at 25 °C. The *46279*, *46282*, *34597* and *34598 UAS*-RNAi *mfl*-silencing lines were from the VDRC RNAi collection [25]. vg^{BE}*–GAL4* and *MS1096–GAL4* strains were kindly provided by S. Cavicchi (University of Bologna, Italy). We also used *ap–GAL4*, *en–GAL4*, *nub–GAL4* and the following strains to generate mosaic flies: *hs*FLP1.22; FRT42D, *arm*LacZ, *M(2)l2*/CyO and *hs*FLP1.22; FRT42D, P[Ubi-GFP]/CyO and *hs*FLP1.22, f^{36a}; FRT42D, f^{+}, *M(2)l2*/CyO. For mosaic analyses, we used the mfl^{05} lethal allele [18] recombined into an FRT42D chromosome. All other stocks were obtained from the Bloomington Drosophila Stock Center (Bloomington, IN, USA).

Morphometric wing analysis

For each progeny, young adult males were sampled and wings were dissected, dehydrated in ethanol, and mounted on glasses in lactic acid/ethanol (6 : 5). Images were captured with a Spot digital camera and a Zeiss Axioplan microscope, using × 5 and × 40 magnification. Areas were quantified using PHOTOSHOP CS3 (Adobe Systems Inc., San Jose, CA, USA). At least 20 wings were examined for each genotype.

Mosaic clonal analysis

Mitotic clones homozygous for the lethal mfl^{05} allele were induced by exposing larvae of the appropriate genotypes to 50 min of heat shock at 60 ± 12 h after egg laying (AEL). Wing discs were dissected at 96–120 h AEL, fixed, and analysed for the absence of LacZ or GFP expression in a MicroRadiance (Bio-Rad Laboratories Inc., Hercules, CA, USA) or Zeiss LSM510 confocal microscopes. The areas of mfl^{05} clones were quantified by using an appropriate tool of PHOTOSHOP (Adobe Systems).

Antibody staining

Wing discs were dissected, fixed and immunostained as described in de Celis [56]. Customer rabbit polyclonal antibody against Mfl [24] (Sigma-Aldrich Inc., St. Louis, MO, USA; dilution 1 : 120), mouse monoclonal antibody against Wg (Hybridoma Bank, University of Iowa, Iowa City, IA, USA; dilution 1 : 50), rabbit polyclonal antibodies against PH3 and activated Cas3 (Cell Signaling Tech., Danvers, MA, USA; dilutions 1 : 200 and 1 : 50, respectively) and rabbit polyclonal antibody against β-galactosidase (Cappel, Solon, CA, USA; dilution 1 : 200) were used. Fluorescent secondary antibodies were from Jackson ImmunoResearch and used at a final dilution of 1 : 200. Samples were analysed in a MicroRadiance (Bio-Rad) or Zeiss LSM510 confocal microscope.

RNA analysis

Total RNA was extracted with Tri Reagent (Sigma). For each sample, 1 μg of RNA from was reverse transcribed using QuantiTect Rev.Transcription Kit (Qiagen, Hilden, Germany) and diluted 1 : 10. Quantitative real-time RT-PCR was performed as previously described [57]. Sequences of all utilized primers were designed using PRIMER 3 software (http://frodo.wi.mit.edu) and are available on request. *αTub84B* mRNA was used as endogenous control for sample normalization.

Acknowledgements

We acknowledge the VDRC (Vienna Drosophila RNAi Center) for providing the *mfl*-silencing strains. The authors are grateful to A. Angrisani for collaborative support and helpful discussions, and to A. Monaco for contributing to *Drosophila* rearing. J. F. de Celis is supported by a grant (BFU2006-06501) from the Spanish Ministry of Education and Science.

References

1 Meier UT (2005) The many facets of H/ACA ribonucleoproteins. *Chromosoma* **114**, 1–14.
2 Ruggero D, Grisendi S, Piazza F, Rego E, Mari F, Rao PH, Cordon-Cardo C & Pandolfi PP (2003) Dyskeratosis congenita and cancer in mice deficient in ribosomal RNA modification. *Science* **299**, 259–262.
3 Yoon A, Peng G, Brandenburger Y, Zollo O, Xu W, Rego E & Ruggero D (2006) Impaired control of IRES-mediated translation in X-linked dyskeratosis congenita. *Science* **312**, 902–906.
4 Gu BW, Bessler M & Mason PJ (2008) A pathogenic dyskerin mutation impairs proliferation and activates a DNA damage response independent of telomere length in mice. *Proc Natl Acad Sci USA* **105**, 10173–10178.
5 Meier UT & Blobel G (1994) NAP57, a mammalian nucleolar protein with a putative homolog in yeast and bacteria. *J Cell Biol* **127**, 1505–1514.
6 Kirwan M & Dokal I (2009) Dyskeratosis congenita, stem cells and telomeres. *Biochim Biophys Acta* **1792**, 371–379.
7 Kiss T (2002) Small nucleolar RNAs: an abundant group of noncoding RNAs with diverse cellular functions. *Cell* **109**, 145–148.
8 Bachellerie JP, Cavaillé J & Hüttenhofer A (2002) The expanding snoRNA world. *Biochimie* **84**, 775–790.
9 Ender C, Krek A, Friedlander MR, Beitzinger M, Weinmann L, Chen W, Pfeffer S, Rajewsky N & Meister G (2008) A human snoRNA with microRNA-like functions. *Mol Cell* **32**, 519–528.
10 Saraiya AA & Wang C (2008) snoRNA, a novel precursor of microRNA in Giardia lamblia. *PLoS Pathog* **4**, e1000224.
11 Taft RJ, Glazov EA, Lassmann T, Hayashizaki Y, Carninci P & Mattick JS (2009) Small RNAs derived from snoRNAs. *RNA* **15**, 1233–1240.
12 Politz JC, Hogan EM & Pederson T (2009) MicroRNAs with a nucleolar location. *RNA* **15**, 1705–1715.
13 Scott MS, Avolio F, Ono M, Lamond AI & Barton GJ (2009) Human miRNA precursors with box H/ACA snoRNA features. *PLoS Comput Biol* **5**, e1000507.
14 Cohen SB, Graham ME, Lovrecz GO, Bache N, Robinson PJ & Reddel RR (2007) Protein composition of catalytically active human telomerase from immortal cells. *Science* **315**, 1850–1853.
15 Heiss NS, Knight SW, Vulliamy TJ, Klauck SM, Wiemann S, Mason PJ, Poustka A & Dokal I (1998) X-linked dyskeratosis congenita is caused by mutations in a highly conserved gene with putative nucleolar functions. *Nat Genet* **19**, 32–38.
16 Knight SW, Heiss NS, Vulliamy TJ, Aalfs CM, McMahon C, Richmond P, Jones A, Hennekam RC, Poustka A, Mason PJ *et al.* (1999) Unexplained aplastic anaemia, immunodeficiency, and cerebellar hypoplasia (Hoyeraal–Hreidarsson syndrome) due to mutations in the dyskeratosis congenita gene, DKC1. *Br J Haematol* **107**, 335–339.
17 Phillips B, Billin AN, Cadwell C, Buchholz R, Erickson C, Merriam JR, Carbon J & Poole SJ (1998) The Nop60B gene of Drosophila encodes an essential nucleolar protein that functions in yeast. *Mol Gen Genet* **260**, 20–29.
18 Giordano E, Peluso I, Senger S & Furia M (1999) minifly, a Drosophila gene required for ribosome biogenesis. *J Cell Biol* **144**, 1123–1133.
19 Grewal SS, Li L, Orian A, Eisenman RN & Edgar BA (2005) Myc-dependent regulation of ribosomal RNA synthesis during Drosophila development. *Nat Cell Biol* **7**, 295–302.
20 Alawi F & Lee MN (2007) DKC1 is a direct and conserved transcriptional target of c-MYC. *Biochem Biophys Res Commun* **362**, 893–898.
21 Gallant P (2009) Drosophila Myc. *Adv Cancer Res* **103**, 111–144.
22 Eilers M & Eisenman RN (2008) Myc's broad reach. *Genes Dev* **22**, 2755–2766.
23 Louis EJ (2002). Are Drosophila telomeres an exception or the rule? *Genome Biol* **3**, REVIEWS 0007.1–0007.6.
24 Riccardo S, Tortoriello G, Giordano E, Turano M & Furia M (2007) The coding/non-coding overlapping architecture of the gene encoding the Drosophila pseudouridine synthase. *BMC Mol Biol* **8**, 8–15.
25 Dietzl G., Chen D., Schnorrer F., Su K. C., Barinova Y., Fellner M., Gasser B., Kinsey K., Oppel S., Scheiblauer S. *et al.* (2007) A genome-wide transgenic RNAi library for conditional gene inactivation in Drosophila. *Nature* **448**, 151–156.
26 Sparrow JC (1978) Melanotic 'tumours'. In *The Genetics and Biology of Drosophila*, Vol. 2b (Ashburner M & Wright TRF eds). 277-313. New York, Academic-Press.
27 Watson KL, Johnson TK & Denell RE (1991) Lethal(1) aberrant immune response mutations leading to melanotic tumor formation in Drosophila melanogaster. *Dev Genet* **12**, 173–187.
28 Milán M, Diaz-Benjumea FJ & Cohen SM (1998) Beadex encodes an LMO protein that regulates Apterous LIM-homeodomain activity in Drosophila wing development: a model for LMO oncogene function. *Genes Dev* **12**, 2912–2920.
29 Martín FA & Morata G (2006) Compartments and the control of growth in the Drosophila wing imaginal disc. *Development* **133**, 4421–4426.
30 Klein T (2001) Wing disc development in the fly: the early stages. *Curr Opin Genet Dev* **11**, 470–475.
31 Tabata T (2001) Genetics of morphogen gradients. *Nat Rev Genet* **2**, 620–630.

32 Morata G & Ripoll P (1975) Minutes: mutants of drosophila autonomously affecting cell division rate. *Dev Biol* **42**, 211–221.
33 Lambertsson A (1998) The Minute genes in Drosophila and their molecular functions. *Adv Genet* **38**, 69–134.
34 Herranz H & Milán M (2006) Notch and affinity boundaries in Drosophila. *Bioessays* **28**, 113–116.
35 Rafel N & Milán M (2008) Notch signalling coordinates tissue growth and wing fate specification in Drosophila. *Development* **135**, 3995–4001.
36 Mohit P, Bajpai R & Shashidhara LS (2003) Regulation of Wingless and Vestigial expression in wing and haltere discs of Drosophila. *Development* **130**, 1537–1547.
37 Lai EC, Tam B & Rubin GM (2005) Pervasive regulation of Drosophila Notch target genes by GY-box-, Brd-box-, and K-box-class microRNAs. *Genes Dev* **19**, 1067–1080.
38 Sieron P, Hader C, Hatina J, Engers R, Wlazlinski A, Muller M & Schulz WA (2009) *DKC1* overexpression associated with prostate cancer progression. *Br J Cancer* **101**, 1410–1416.
39 Xu T & Rubin GM (1993) Analysis of genetic mosaics in developing and adult Drosophila tissues. *Development* **117**, 1223–1237.
40 Giordano E, Rendina R, Peluso I & Furia M (2002) RNAi triggered by symmetrically transcribed transgenes in Drosophila melanogaster. *Genetics* **160**, 637–648.
41 Johnston LA (2009) Competitive interactions between cells: death, growth, and geography. *Science* **324**, 1679–1682.
42 Tyler DM, Li W, Zhuo N, Pellock B & Baker NE (2007) Genes affecting cell competition in Drosophila. *Genetics* **175**, 643–657.
43 de la Cova C, Abril M, Bellosta P, Gallant P & Johnston LA (2004) Drosophila myc regulates organ size by inducing cell competition. *Cell* **117**, 107–116.
44 Moreno E & Basler K (2004) dMyc transforms cells into super-competitors. *Cell* **117**, 117–129.
45 Johnston LA, Prober DA, Edgar BA, Eisenman RN & Gallant P (1999) Drosophila myc regulates cellular growth during development. *Cell* **98**, 779–790.
46 Hart K, Klein T & Wilcox M (1993) A Minute encoding a ribosomal protein enhances wing morphogenesis mutants. *Mech Dev* **43**, 101–110.
47 Enerly E, Larsson J & Lambertsson A (2003) Silencing the Drosophila ribosomal protein L14 gene using targeted RNA interference causes distinct somatic anomalies. *Gene* **320**, 41–48.
48 Hall LE, Alexander SJ, Chang M, Woodling NS & Yedvobnick B (2004) An EP overexpression screen for genetic modifiers of Notch pathway function in Drosophila melanogaster. *Genet Res* **83**, 71–82.
49 Alexander SJ, Woodling NS & Yedvobnick B (2006) Insertional inactivation of the L13a ribosomal protein gene of Drosophila melanogaster identifies a new Minute locus. *Gene* **368**, 46–52.
50 Cui Z & DiMario PJ (2007) RNAi knockdown of Nopp140 induces Minute-like phenotypes in Drosophila. *Mol Biol Cell* **18**, 2179–2191.
51 Tien AC, Rajan A & Bellen HJ (2009) A Notch updated. *J Cell Biol* **184**, 621–629.
52 Grozdanov PN, Fernandez-Fuentes N, Fiser A & Meier UT (2009). Pathogenic Nap57 mutations decrease ribonucleoprotein assembly in dyskeratosis congenita. *Hum Mol Genet* **18**, 4546–4551.
53 Moreno E (2008) Is cell competition relevant to cancer? *Nat Rev Cancer* **8**, 141–147.
54 Oliver ER, Saunders TL, Tarlé SA & Glaser T (2004) Ribosomal protein L24 defect in belly spot and tail (Bst), a mouse Minute. *Development* **131**, 3907–3920.
55 He J, Navarrete S, Jasinski M, Vulliamy T, Dokal I, Bessler M & Mason PJ (2002) Targeted disruption of Dkc1, the gene mutated in X-linked dyskeratosis congenita, causes embryonic lethality in mice. *Oncogene* **21**, 7740–7744.
56 de Celis JF (1997) Expression and function of decapentaplegic and thick veins during the differentiation of the veins in the Drosophila wing. *Development* **124**, 1007–1018.
57 Tortoriello G, Accardo MC, Scialò F, Angrisani A, Turano M & Furia M (2009) A novel Drosophila antisense scaRNA with a predicted guide function. *Gene* **436**, 56–65.

Supporting information

The following supplementary material is available:
Fig. S1. Quantitative variations in *mfl* transcript levels after ubiquitous RNAi silencing.
Fig. S2. Adult wing phenotype displayed by *46282/MS1096–GAL4* flies.
Fig. S3. A survey of phenotypes obtained with the *34598* and *34597 mfl*-silencing lines.
Fig. S4. A canonical Brd-box sequence at the 3′-UTR of the *mfl* 2.0 and 2.2 kb mRNAs.
Fig. S5. D/V and A/P ratios of actively dividing cells in *46282/ap–GAL4*-silenced and *46282/en–GAL4*-silenced discs.

This supplementary material can be found in the online version of this article.

Please note: As a service to our authors and readers, this journal provides supporting information supplied by the authors. Such materials are peer-reviewed and may be re-organized for online delivery, but are not copy-edited or typeset. Technical support issues arising from supporting information (other than missing files) should be addressed to the authors.